Annals of Botany **107**: 843–853, 2011
doi:10.1093/aob/mcr005, available online at www.aob.oxfordjournals.org

ANNALS OF BOTANY
Founded 1887

PART OF A SPECIAL ISSUE ON GROWTH AND ARCHITECTURAL MODELLING

Three-dimensional distribution of vessels, passage cells and lateral roots along the root axis of winter wheat (*Triticum aestivum*)

Haiwen Wu[1], Marc Jaeger[2], Mao Wang[3], Baoguo Li[1] and Bao Gui Zhang[1,*]

[1]*Key Laboratory of Plant–Soil Interactions, College of Resources and Environmental Sciences, China Agricultural University, 100193 Beijing, China,* [2]*CIRAD-AMAP, EPI Digiplante, Bd de la Lironde 34398, Montpellier cedex 5, France and* [3]*College of Biological Sciences, China Agricultural University, 100193 Beijing, China*
** For correspondence. E-mail zhangbg@cau.edu.cn*

Received: 16 July 2010 Returned for revision: 21 October 2010 Accepted: 23 November 2010 Published electronically: 2 February 2011

• *Background and Aims* The capacity of a plant to absorb and transport water and nutrients depends on anatomical structures within the roots and their co-ordination. However, most descriptions of root anatomical structure are limited to 2-D cross-sections, providing little information on 3-D spatial relationships and hardly anything on their temporal evolution. Three-dimensional reconstruction and visualization of root anatomical structures can illustrate spatial co-ordination among cells and tissues and provide new insights and understanding of the interrelation between structure and function.
• *Methods* Classical paraffin serial-section methods, image processing, computer-aided 3-D reconstruction and 3-D visualization techniques were combined to analyse spatial relationships among metaxylem vessels, passage cells and lateral roots in nodal roots of winter wheat (*Triticum aestivum*).
• *Key Results* 3-D reconstruction demonstrated that metaxylem vessels were neither parallel, nor did they run directly along the root axis from the root base to the root tip; rather they underwent substitution and transition. Most vessels were connected to pre-existent or newly formed vessels by pits on their lateral walls. The spatial distributions of both passage cells and lateral roots exhibited similar position-dependent patterns. In the transverse plane, the passage cells occurred opposite the poles of the protoxylem and the lateral roots opposite those of the protophloem. Along the axis of a young root segment, the passage cells were arranged in short and discontinuous longitudinal files, thus as the tissues mature, the sequence in which the passage cells lose their transport function is not basipetal. In older segments, passage cells decreased drastically in number and coexisted with lateral roots. The spatial distribution of lateral roots was similar to that of the passage cells, mirroring their similar functions as lateral pathways for water and nutrient transport to the stele.
• *Conclusions* With the 3-D reconstruction and visualization techniques developed here, the spatial relationships between vessels, passage cells and lateral roots and the temporal evolution of these relationships can be described. The technique helps to illustrate synchronization and spatial co-ordination among the root's radial and axial pathways for water and nutrient transport and the interdependence of structure and function in the root.

Key words: Winter wheat, *Triticum aestivum*, metaxylem vessel, passage cell, lateral root, 3-D reconstruction, 3-D visualization, spatial co-ordination, positional relationship.

INTRODUCTION

In higher plants, roots carry out the important functions of acquiring water and soil nutrients and transporting these upwards to the aerial parts. These functions are closely related to their anatomical structure; soil water and nutrients first move radially through several concentric layers of the epidermis, cortex and endodermis before entering the central cylinder of the root where they are transported longitudinally via the xylem vessels to the plant's aerial parts (Steudle and Peterson, 1998). The spatial organization and co-ordination of all these structures are essential for the continuity of the radial and longitudinal pathways to ensure efficient absorption and transport of water and solutes. Until now, descriptions of root internal structure have commonly been limited to 2-D cross-sections, with little systematic and quantitative information available in three dimensions. For example, in plant physiological textbooks, 3-D illustration of the structures are usually schematic.

Monocots have no secondary growth, so all their structures must be pre-built in the early stages of development. As a consequence, they must evolve during early root development as they accommodate the increasing demands of absorption and transport as the root matures. As root development progresses basipetally, the temporal evolution of root anatomical structure is reflected in a spatial evolution along the root axis from the apex (root tip) to the base (where the root joins the stem). Thus 3-D reconstruction and visualization illustrate not only spatial relationships between the various root tissues, but they also describe the temporal evolution of these relationships to provide new insights into models that summarize our understanding of plant structure and function. As far as is known, no 3-D reconstructions of root anatomical structure and function have been reported for wheat.

A plant's root system is usually buried within the soil matrix, which prevents direct and continuous observation, so that the roots can fairly be described as the 'hidden half' of a plant. As a result, three-dimensional reconstruction studies of roots began much later than similar studies on shoots. Although 3-D reconstruction on roots has become more widespread in recent years, most have used sophisticated and expensive equipment and focused on root architecture, using, for example, computed tomography (CT) scan technology (Lontoc-Roy *et al.*, 2004, 2005; Kaestner *et al.*, 2006; Tracy *et al.*, 2010) and laser scanners (Fang *et al.*, 2009). X-ray devices have been used for the plant internal structure (Simionovici *et al.*, 2001; Stuppy *et al.*, 2003) and confocal laser scanning microscopy (CLSM) for embryonic root tip cells (Truernit *et al.*, 2008). Three-dimensional reconstruction and visualization is a promising tool for studying the spatial relationships among structures. There are reports of its application at the plant organ (Lee *et al.*, 2006; Zhu *et al.*, 2008) and cell level (Eils and Athale, 2003; Truernit *et al.*, 2008). It has also been applied to stem xylem vessels (Lin *et al.*, 1997; Bardage, 2001; Mayo *et al*, 2010), to phloem (Truernit *et al.*, 2008) and even to the intercellular void network in arabidopsis seeds (Cloetens *et al.*, 2006). Studies using these techniques have also been carried out on cellular dynamics (de Reuille *et al.*, 2005) and on the positions of chromosomes (Gerlich *et al.*, 2003). But the high cost of image acquisition has restricted the broader application of 3-D reconstruction to root studies, including in monocots such as wheat.

In the present study, a low-cost computer-aided 3-D reconstruction and visualization technique was developed based on serial sections obtained using classical paraffin embedding and microtome techniques. This allowed rapid 3-D visualization and quantitative analysis. The spatial arrangements of metaxylem vessels, passage cells and lateral roots were analysed on nodal roots of winter wheat (*Triticum aestivum*) to illustrate the spatial relationship between these anatomical structures and their temporal evolution along the root axis.

MATERIALS AND METHODS

Plant materials

Winter wheat (*Triticum estivum* L.) seedlings were cultivated in a growth chamber. Plants were grown in PVC columns of sand and watered regularly with a nutrient solution formulated for monocotyledons (Romheld and Marschner, 1986). When the plants had grown for about 1 month, seedlings were selected which have five or six leaves on the main stem and 15- to 20-cm-long nodal roots with lateral roots and relatively straight axes. From these plants, roots were selected randomly. Segments with lateral roots were excised along the nodal root axis in the direction from root base (basal) to root tip (distal). On the root segments, lateral roots were trimmed to length of about 1 cm – curvature caused by gravitropism allowed distinction of the basal and distal ends of the root segments. Segment samples were fixed in formalin : acetic acid : alcohol (90 : 5 : 5, v/v/v). After dehydration and embedding in paraffin wax, serial cross-sections were cut (http://homepages.gac.edu/~cellab/chpts/chpt2/intro2.html) using a microtome in the direction from base to tip. Sections were stained with safranin-fast green (Johansen, 1940), which dyed the lignified secondary cell walls of the vessels and the endodermal cells red and the living cells green.

Image acquisition

Each section was viewed under an Olympus BX-51 optical microscope with a DP-70 digital camera connected to a personal computer. Initially, the serial sections were cut to 10 μm thick (the usual thickness for study of root structure). As the technique was developed, it was found that several slice images could be skipped without affecting the subsequent image processing, such as alignment. This meant serial sections could be cut thicker and some images could be skipped, thus the maximum thickness setting of the microtome (25 μm) was chosen for later work. The corresponding coloured images of the root stele were stored in high-resolution tif files, a format with no loss of definition during saving. The serial images of each set were taken using exactly the same protocol for colouration, concentration, light intensity, zoom factor, image resolution and pixel size.

Main steps of 3-D reconstruction using the specific program

The serial images of a given segment were converted to grey scale (Fig. 1A) and loaded into the volume imaging software AMBIOS (Analysis and Modeling of Biological Systems, developed by CIRAD-AMAP; http://amap.cirad.fr/en/mia_theme2.php). The image processing protocol involved serial image alignment, registration and 3-D reconstruction. Image alignment was performed according to the protocol described by the authors of the AMBIOS protocol (developed on human and rat embryos; Prudhomme *et al.*, 1999). The detailed operation and process are described by Wu *et al.* (2009). Taking vessels as an example, the main steps can be summarized as follows.

First, the image labels (micrometres per pixel) were calibrated to establish the measurement scale. Cell edges were then computed after setting up the appropriate parameters (Fig. 1B). Next, an image in the middle of the series was selected as reference edge image. Succeeding and anteceding images then rotated and translated automatically to match the reference edges (Fig. 1C, D) until the images no longer matched. Another reference was then chosen from the aligned images and the process was repeated until the full image set was well aligned. Then, cell lumens were detected automatically throughout the full image set by a simple threshold test. Vessels of interest were selected by clicking on the vessel lumen and coded with one of several colours selected from a predefined table (Fig. 1E). Thereafter, the system automatically propagated these colours up and down to the same structures in the aligned segment volume. The last step was to remove the background colours (Fig. 1F) and to perform the 3-D visualization.

Vessel section areas, average diameters, volume of individual vessels, the central point and co-ordinate matrix, and colour information could be generated automatically. From these features, a virtual vessel geometrical system was constructed. This model was then described using VRML (Virtual Reality Modeling Language; Hartman and Wernecke, 1996), a 3-D web language, allowing real-time

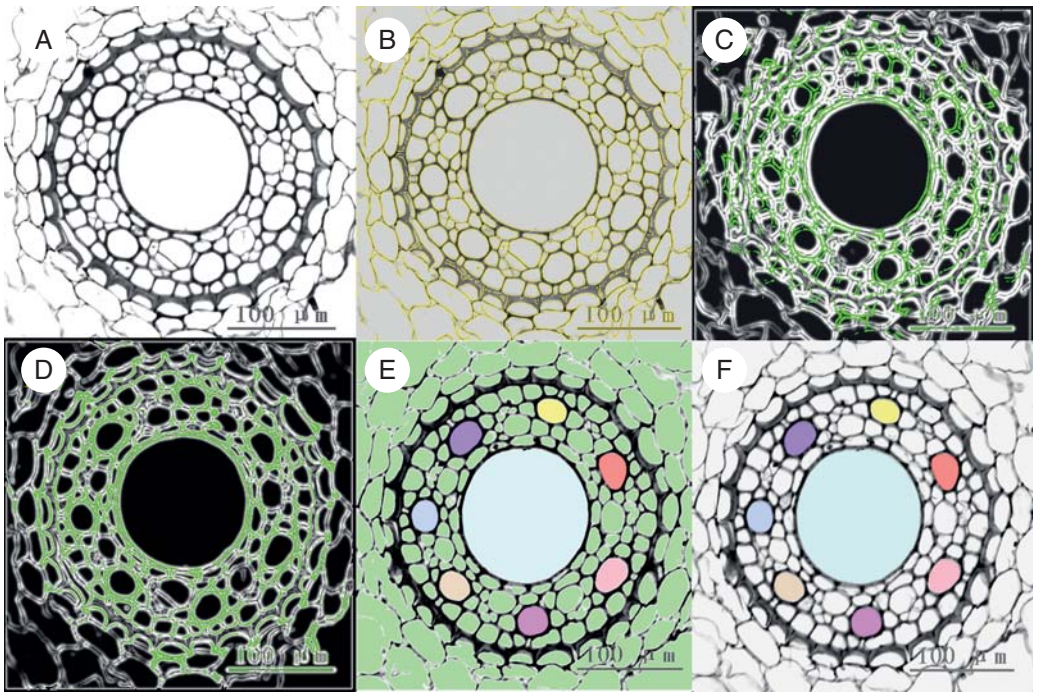

FIG. 1. Main steps of image processing in the 3-D reconstruction program (xylem vessels as an example). (A) Colour images of the root stele are converted to grey-scale images, then loaded into the AMBIOS program and adjusted to optimal brightness and definition. (B) Edges of cells are computed by the program after setting up the appropriate parameters. The yellow curves are the computed cell edges (coinciding with the cell walls). (C) An image in the middle of the series is defined as the reference image and the cell edges are coloured green. A succeeding or anteceding image (cell edges coloured white) is superimposed. The image does not match the reference image until the green and the white lines coincide. (D) Images are rotated and translated to best match the reference. (E) On the image in the middle of the series, all the cells are filled with green (default colour of the system). Xylem vessels in the reference image to be reconstructed are selected and their lumens are manually filled with different colours. The vessel colour registrations are then propagated to the other aligned images. (F) The background colour, no longer necessary, is removed leaving the selections (vessels) for 3-D-reconstruction and visualization.

3-D views. Because the same protocol was used in all samples, the results could be directly compared.

3-D distribution of lateral roots and passage cells

Both lateral roots and passage cells have specific positions in the wheat root. In the cross-sections, lateral roots are located opposite the poles of the protophloem and passage cells are opposite those of the protoxylem. Therefore the position of the phloem was used as a reference to label the location of the lateral roots, and similarly the position of the protoxylem for the passage cells. Those positions were expressed in a classical, cylindrical co-ordinate system.

A phloem bundle was selected arbitrarily as the starting point and the other phloem bundles (lateral roots) were labelled clockwise according to their radial angle (radians) relative to the start point (Fig. 2). In the longitudinal files, the positions of the lateral roots were noted by their distances to the base of the segment. Thus the 3-D position of a lateral root was determined by its radial angle in transverse section and its longitudinal distance to the segment base.

Radial positions of passage cells were labelled in the same way, except that the starting point was a protoxylem pole instead of a phloem pole.

A chi-square test was use to check if the distribution of the lateral roots or passage cells differed significantly from being random.

RESULTS

3-D reconstruction and visualization of root anatomical structure

As shown in Fig. 3, the relative sizes and 3-D extension of vessels were clearly illustrated. Observations could be made directly from the top (Fig. 3A, C, F), side (Fig. 3E) and from a sectional view (Fig. 3B). These views could also be combined (Fig. 3D). Furthermore, the reconstruction provided a longitudinal profile of the root axis (Fig. 3H) based on the cross-sections, and tracking of the transition of individually selected cells (the xylem vessels in this case). A synthetic 3-D image reconstructed by VRML based on serial areas and the co-ordinate matrixes of the centre of gravity could also be achieved (Fig. 3G) and used to combine the separate parts (Fig. 4A).

Evolution of the metaxylem vessels along the root axis

The transverse sections of the nodal root stele showed two types of vessels: (1) wide, central metaxylem vessels in small numbers with diameters of 40–50 μm; and (2) numerous smaller peripheral protoxylem vessels with diameters of 10–15 μm (Figs 4A and 5a, b).

The transition of metaxylem vessels was clearly illustrated with the 3-D reconstruction and visualization technique (Fig. 4A). The metaxylem vessels did not run in a straightforward manner through the root axis from base to tip; instead, newly differentiated vessels were connected to the old ones

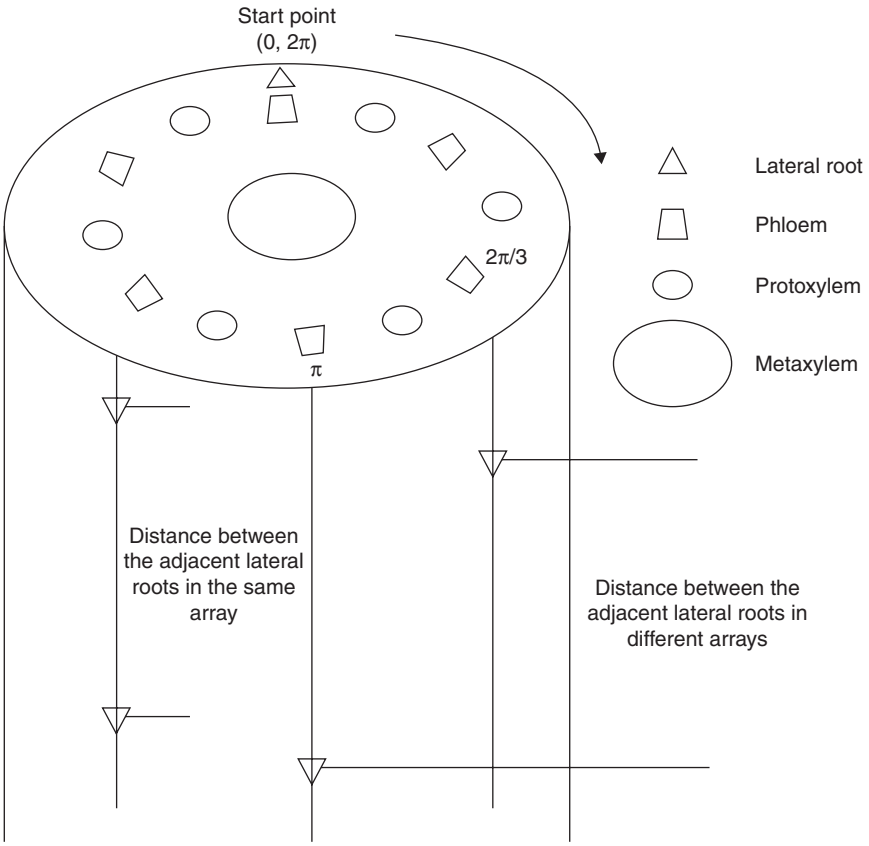

FIG. 2. Representations of 3-D distribution of lateral roots. Since lateral roots originate from the pericycle cells out of the phloem, the phloem bundles are considered as the reference for the lateral roots. One phloem bundle is arbitrarily taken as the starting point. The others are labelled clockwise, being identified by their radial angles from the start point. In the longitudinal direction, the position of a lateral root is noted by its distance from the base of the segment. Thus the 3-D position of any lateral root is defined by a radial angle in transverse section and the axial distance to the segment base.

by their lateral walls (Fig. 4B). Along the root axis, the number of metaxylem vessels decreased from the proximal (root base) to the distal (root tip) end (Fig. 4C1, C2), so that not all vessel elements in the proximal end connected directly to the newly formed ones in the distal end (Fig. 4A, vessel 05).

3-D-distribution of passage cells and lateral roots

In the transverse plane, passage cells occurred adjacent to the poles of the protoxylem (Fig. 5a, b). The pericycle cells between the passage cells and protoxylem poles were much smaller than the others (Figs 5A, B and 6A1, A2). In some cases, they were so small and abnormal in shape that they appeared as intercellular spaces on the inner side of the passage cells (Fig. 6A3).

The frequency of passage cells decreased with increasing distance from the root apex. For example, at a point 1·5 cm from the root tip (where lateral roots had not yet appeared) four to six passage cells appeared in any section (Fig. 5b), whereas more basally, at about 3 cm from the root apex, the number of passage cells visible was only about two in most sections, with a maximum of three (Fig. 5a). In older sections (Fig.6A, e.g. at the base of the root and about 14 cm from the tip) where most of the endodermal cells had undergone wall thickening, the maximum number of passage cells in a transverse section was four, with most sections containing none or only one passage cell (Fig. 6A). As mentioned previously, passage cells occurred adjacent to the poles of the protoxylem; thus if the number of protoxylem poles is considered, the rarity of the passage cells in the oldest root sections was even more pronounced because at this position there were 11–15 protoxylem poles, compared with six poles in sections close to the root tip. The 3-D reconstruction and visualization revealed that passage cells were arranged in discontinuous longitudinal files along the root axis. They tended to cluster in one half of the transverse plane over a short distance [Figs 5 (3-D reconstruction of segment B) and 6B]. In the longitudinal direction, passage cells were dispersed radially (Fig. 6B). In one particular 2-cm root segment, there were 37 passage cells belonging to 11 files (Fig. 6B).

The lateral root arrangement along the root axis could be illustrated using 3-D reconstruction. On any particular transverse section, lateral roots were positioned adjacent to the protophloem poles and were oriented towards the metaxylem vessels (Fig. 7A). Longitudinally, the distribution of lateral roots along the axis was very similar to that of the passage cells. Over short distances they were assembled on one side of the transverse plane (Fig. 7A). Chi-square tests showed that the radial distribution of lateral roots was not random

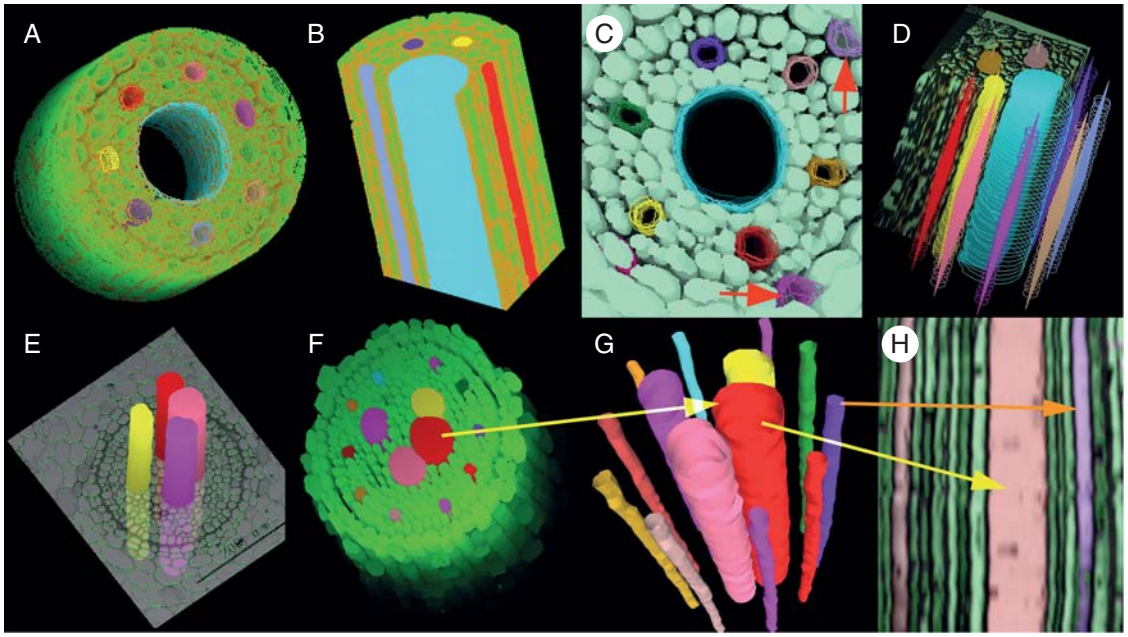

FIG. 3. Various 3-D views of the reconstructed root tissues. The green colour represents living cells in the stele and other colours represent vessels. (A) The 3-D reconstruction of the stele with the centre metaxylem vessel shown as open. The thickened cell walls of the endodermis cells are coloured brown. (B) Two perpendicular cutting profiles on the reconstructed stele, with narrow protoxylem vessels at the periphery and a wide metaxylem vessel in the centre. (C) A 3-D reconstruction of the stele with six protoxylem vessels and one central metaxylem vessel. Note passage cells (red arrows) opposite the protoxylem poles. (D) Compound views of vessels including a cut view (note the metaxylem vessel in blue) and the view of the edges as wireframes. Solid forms inside the wireframes indicate the centre of gravity of the vessels. (E) Reconstructed metaxylem vessels running through a cross-section show their relative position in the stele. (F) Reconstructed stele of a nodal root. Large vessels are metaxylem and narrow ones are protoxylem. Note that there are more than one metaxylem vessel in the stele. (G) Reconstruction and visualization of isolated metaxylem and protoxylem vessels by VRML file based on the same serial cross-sections as in (F). (H) Reconstructed longitudinal profile of the vessels based on the same serial cross-sections as in (F). Arrows with the same colour in (F), (G) and (H) indicate the same vessels.

($n = 10$), although in longer segments there was a tendency towards a more random distribution (Fig. 7B). Moreover, they were located on the convex side of the mother roots (Fig. 7A).

DISCUSSION

As far as is known, the 3-D spatial distribution of passage cells has not been described previously in wheat. Waduwara *et al.* (2008) reported that in young onion roots, passage cells were arranged in long continuous files, two or three cells wide, alternating with non-passage cell files. The present results for the 3-D arrangement of passage cells in wheat differ from this description. Root cells and tissues generally differentiate and mature in a basipetal direction so that endodermal cells losing their 'passage' function can be considered as merely progressing in their development (Peterson and Enstone, 1996). The passage cells are arranged in longitudinally discontinuous files opposite the protoxylem poles (Figs 5 and 6). Within the same file, passage cells (considered as less differentiated) may occur farther away from the root apex than non-passage cells. This implies that the fate of endodermal cells is not determined by their own developmental programme; instead, it is conditioned by their position, as suggested also by their regular proximity to the protoxylem poles.

The development of passage cells into non-passage cells and also xylem vessel differentiation both involve secondary wall deposition (Ma and Peterson, 2001; Lux and Luxová, 2003; Waduwara *et al.*, 2008), and both lateral root initiation and vascular patterning are regulated by auxin (Aloni and Zimmermann, 1983; Aloni, 1992, 2004; Casimiro *et al.*, 2001; Aloni *et al.*, 2006; De Smet *et al.*, 2006, 2007; Grieneisen *et al.*, 2007; Lucas *et al.*, 2008). This suggests that the spatial co-ordination of passage cells, lateral roots and xylem vessels could be regulated by a common mechanism, and this might explain the origins of the spatial co-ordination in root anatomical structure that constitutes the radial and axial pathway for water and nutrient transport.

Ecological and physiological relevance of xylem vessel transition

The 3-D reconstruction and visualization of root anatomical structure demonstrated that metaxylem vessels were neither parallel, nor do they run throughout the root axis from base to tip in a straightforward manner. Instead, they underwent substitution and transition with numbers decreasing apically along the axis (Fig. 4). These results differ from the descriptions of a 'pipe' model in which all conduits run in parallel within each rank, with constant numbers and diameters (West *et al.*, 1999; Enquist *et al.*, 2000). But the present results are in general agreement with the hormonal mechanism proposed by Aloni (1992, 2004), who stated that metaxylem vessels were induced by polar IAA streams. Thus along the plant axis, the gradual and continuous increase in vessel width and decrease in vessel density with increasing distance

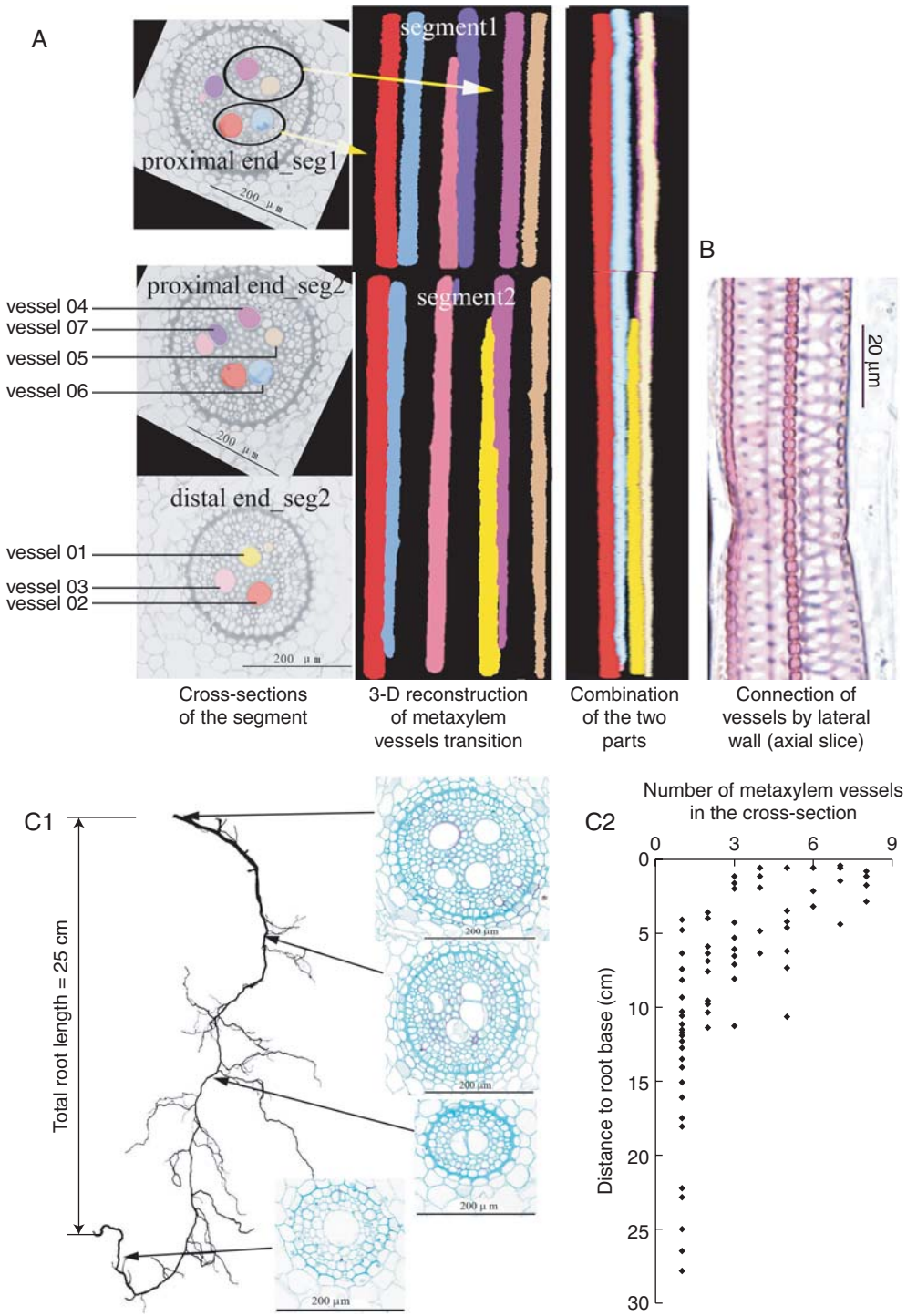

FIG. 4. 3-D visualization underlines the substitution and transitions of metaxylem vessels along the wheat nodal root axis. (A) Cross-sections of the stele and 3-D reconstructions and visualization of the vessels. As the presence of a lateral root interrupts the progressive change of anatomical structure of the main root, the 3-D reconstruction and visualization of the root segment have to be performed separately on two parts: segment 1 towards the root base and segment 2 to the root apex. On the left are presented the cross-sections of two root segments: proximal end (towards the root base) of segment 1, proximal end of segment 2 and distal end (towards the root apex) of segment 2. The images in the middle of (A) are 3-D reconstructions in each segment, illustrating the transition of vessels along the root segment. Vessels in the segments can be distinguished one from the other by colours, note that vessel 07 (violet) that was visible in segment 1 and in the proximal end of segment 2, did not appear in the distal end of segment 2, meanwhile the yellow one (vessel 01) was newly formed, as it does not occur in segment 1. On the right of (A) is a side view of the two segments performed by section interpolation described within a VRML file. (B) Longitudinal section showing two vessels are connected by pits on their lateral walls. (C1) Evolution of the metaxylem vessels along a nodal root axis. The length of the root is 25 cm. The slice images are taken at each segment indicated by the arrows. The number of metaxylem vessels decreases from root base to root tip. (C2) Evolution of the number of metaxylem vessels along the root axis – data from cross-sections of 12 roots. In most roots, the number of metaxylem vessels decreases to one at 10 cm from the root base.

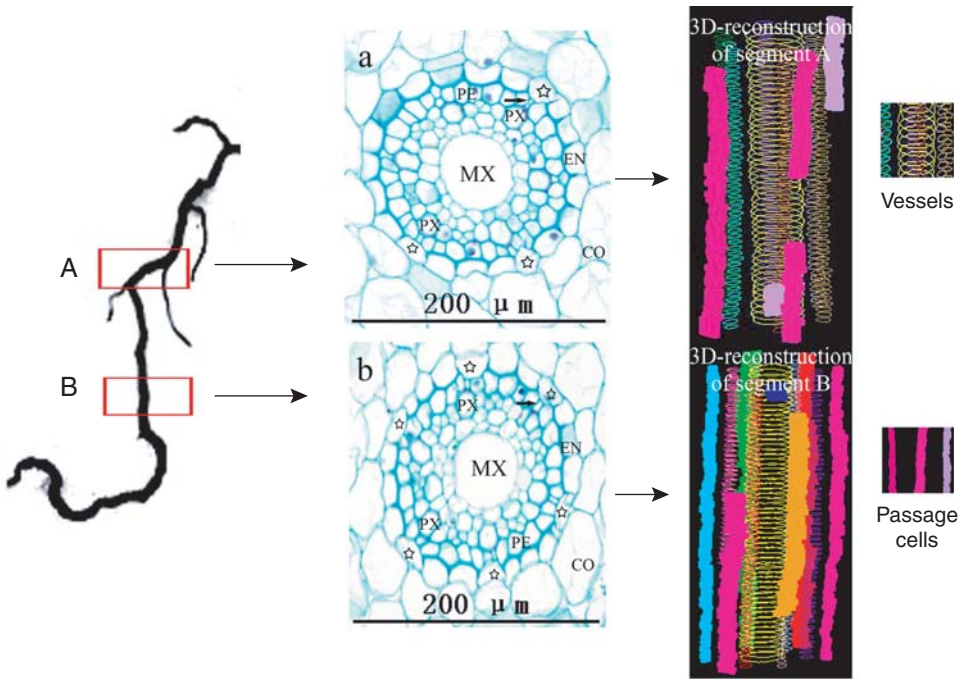

FIG. 5. 3-D arrangement of passage cells on root segments close to the root tip. Left: location of the samples. Root segments about 0·5 cm long were taken at 3-cm intervals (segment A, more proximal to the root base) and 1·5 cm (segment B, more distal) to the root tip, the lengths of the reconstructed segments were 500 μm for segment A and 590 μm for segment B. Middle: cross-sections made on segments A and B, respectively. MX, Metaxylem vessel; PX, protoxylem vessel; CO, cortex; EN, endodermis. Six passage cells (indicated by stars and differing from the other endodermal cells by having non-thickened inner-tangential walls) are in (b) and only three in (a). Note that pericycle cells adjacent to passage cells (indicated by the arrows) are smaller than the others. Right: 3-D-reconstructions of segments A and B showing short non-continuous files of passage cells represented by different colour solid columns surrounding the metaxylem vessels (wireframes).

from the leaves was probably induced by a decreasing gradient of IAA concentration from young leaves to root tips.

About 70–80 % of wheat nodal roots are distributed in the top 20 cm of soil (Ma, 1999) where freeze/thaw and wet/dry cycles are common. These environmental factors increase the risk of embolism, which breaks fluid continuity in the xylem conduits (North, 2004). Occurrence of cavitation in xylem vessels also increases with increasing conduit diameter (Tyree and Ewers, 1991; Sperry and Hacke, 2002). Large numbers and more scattered metaxylem vessels near the root base will therefore help to increase the number of functional conduits in the face of embolism. Moreover, the frequent substitution and transition of xylem vessels could help to limit invasion by pathogenic microorganisms by forcing the fluid to traverse lateral wall connections. Fluctuation in soil temperature and moisture decrease with depth, reducing the risk of embolism in the deeper soil layer. The big centre vessels ensure higher transport efficiency. Thus, the distribution pattern of metaxylem presented here represents a compromise between transport security and transport efficiency.

Temporal evolution and spatial co-ordination of the radial and axial pathways of water and nutrients

Water and ions absorbed from the soil solution by root hairs and the epidermis are transported to the endodermis through an apoplastic pathway that consists of cell walls and intercellular spaces. As a root segment matures, hydrophobic Casparian bands consisting of suberin and/or lignin develop in the radial and anticlinal walls of the endodermis cells and the apoplastic pathway is thus interrupted (Ma and Peterson, 2003). Water and ions such as Ca^{2+} must enter the endodermis symplastically through the membranes lining the outer tangential walls (towards the cortex) and leave the endodermal cells via the membranes lining the inner tangential walls (pericycle side) to join the apoplastic path of the stele. Thus the endodermis should not be considered merely as a barrier to the apoplastic pathway as it also serves as a filter and regulator of water and ion diffusion into the stele, via ATPase pumps and aquaporins located in the membranes of the endodermic cells (Steudle and Peterson, 1998).

With the process of root ageing in the older root segments, suberized lamellae, which are impermeable to water and ions, are deposited on the inner surfaces of some endodermal cell walls. Any bridging of the apoplastic pathway through these cells is completely interrupted, and only a few endodermal cells opposite the protoxylem poles remain as passage cells (Fig. 5). According to Poisseuille's law, the hydraulic conductance of a vessel is proportional to the 4th power of its diameter (Zimmermann, 1983), so it can be speculated that the protoxylem vessels (having much smaller internal diameters than the larger metaxylem vessels) no longer play any significant part in the axial transport of water and nutrients once the metaxylem vessels are mature and functional.

In very old root segments, even if passage cells are still present, their frequency decreases drastically. The radial transport function is taken over by the lateral roots, which break through the endodermal barrier. In the radial plane, lateral roots are directed towards the metaxylem, which facilitates the communication of their vascular system with that of the

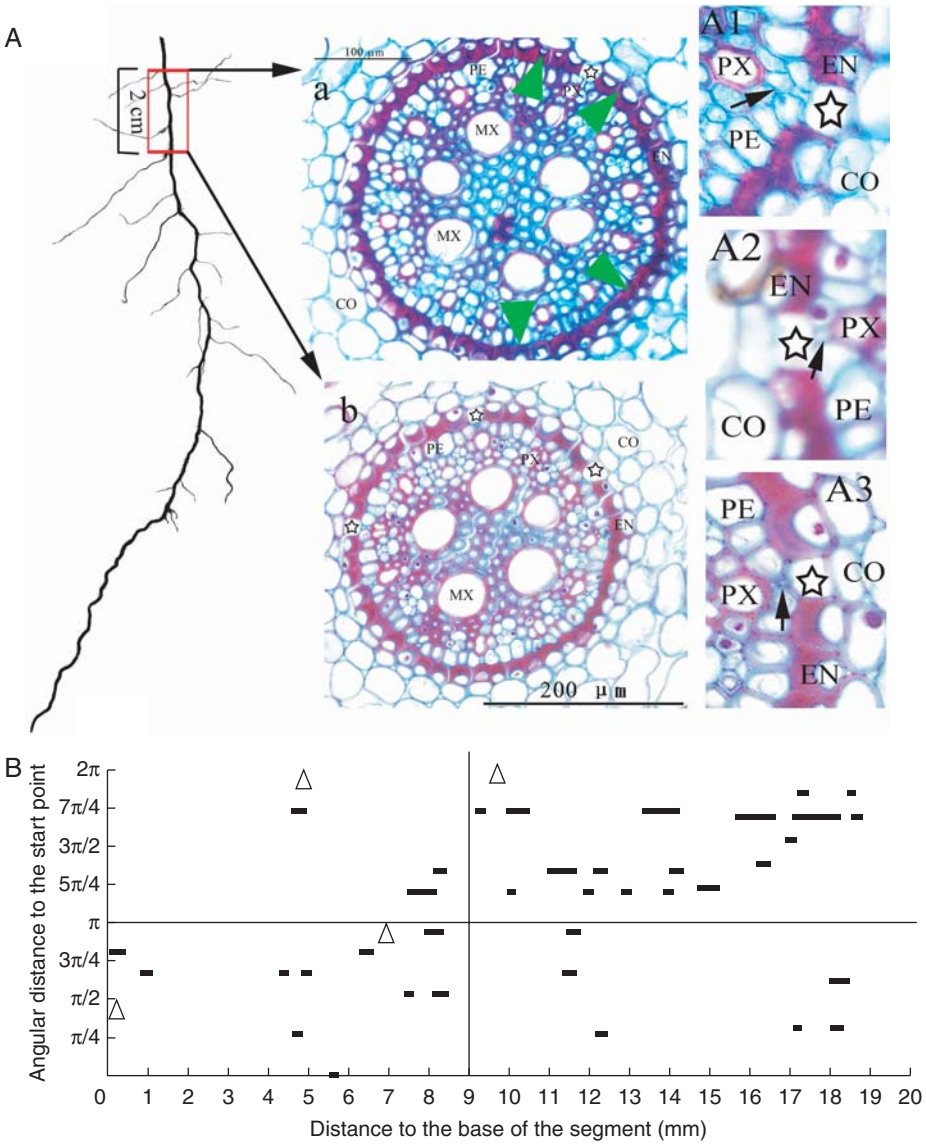

FIG. 6. Distribution of passage cells in an old root segment near the root base. (a) Cross-sections at about 14 cm (a) and 12 cm (b) from the root tip. Note that the passage cells (indicated by stars) are much less frequent in the section taken near the root base (a) than in the section from the more distal position (b). The green arrowheads indicate the radial position of the four lateral roots on the 2-cm-long segment. (A1), (A2) and (A3) are magnifications of portions of selected sections. Several (A1) or one (A2) small pericycle cells (indicated by black arrows) lie between the protoxylem poles and the passage cells. Some of them are very small and look similar to an intercellular space (A3). CO, Cortex; EN, endodermis; PE, pericycle; MX, metaxylem; PX, protoxylem. (B) The longitudinal arrangement of passage cells along the root axis. Passage cells are arranged in short discontinuous files. They tend to cluster in one half of the transverse plane over a short distance (in 0-π for 0–9 mm from the root base; in π-2π for 9–19 mm from the root base). In the longer distance, passage cells seem to disperse radially. Triangles indicate the positions of the lateral roots.

mother roots. It is interesting that lateral roots, which play a similar function in axial transport to the passage cells, also share the same distribution characteristics. Longitudinally, lateral roots and passage cells (or short files of them) are distributed along the parent root axis in a non-random pattern; over short distances they tend to cluster on one side of a transverse plane (Fig. 7A), while over longer distances they tend to be dispersed more uniformly (Fig. 7B). Radially, passage cells and lateral roots lie in proximity to protoxylem or protophloem poles. These results are in general agreement with previous findings for a diversity of other species (Mallory *et al.*, 1970; Dubrovsky *et al.*, 2000). Taken together, this demonstrates close interdependence between anatomical structures and function. For example, it is not surprising that Cholewa and Peterson (2004) found that radioactive Ca^{2+} applied to a root segment near the root apex was not transported to the remainder of the plant, because the endodermis was immature without Casparian bands and protoxylem vessels were not yet functional.

CONCLUSIONS AND PERSPECTIVES

In this study, 3-D reconstruction and visualization were applied to the anatomical structure of winter wheat root. The computer-aided 3-D reconstruction technique presented here

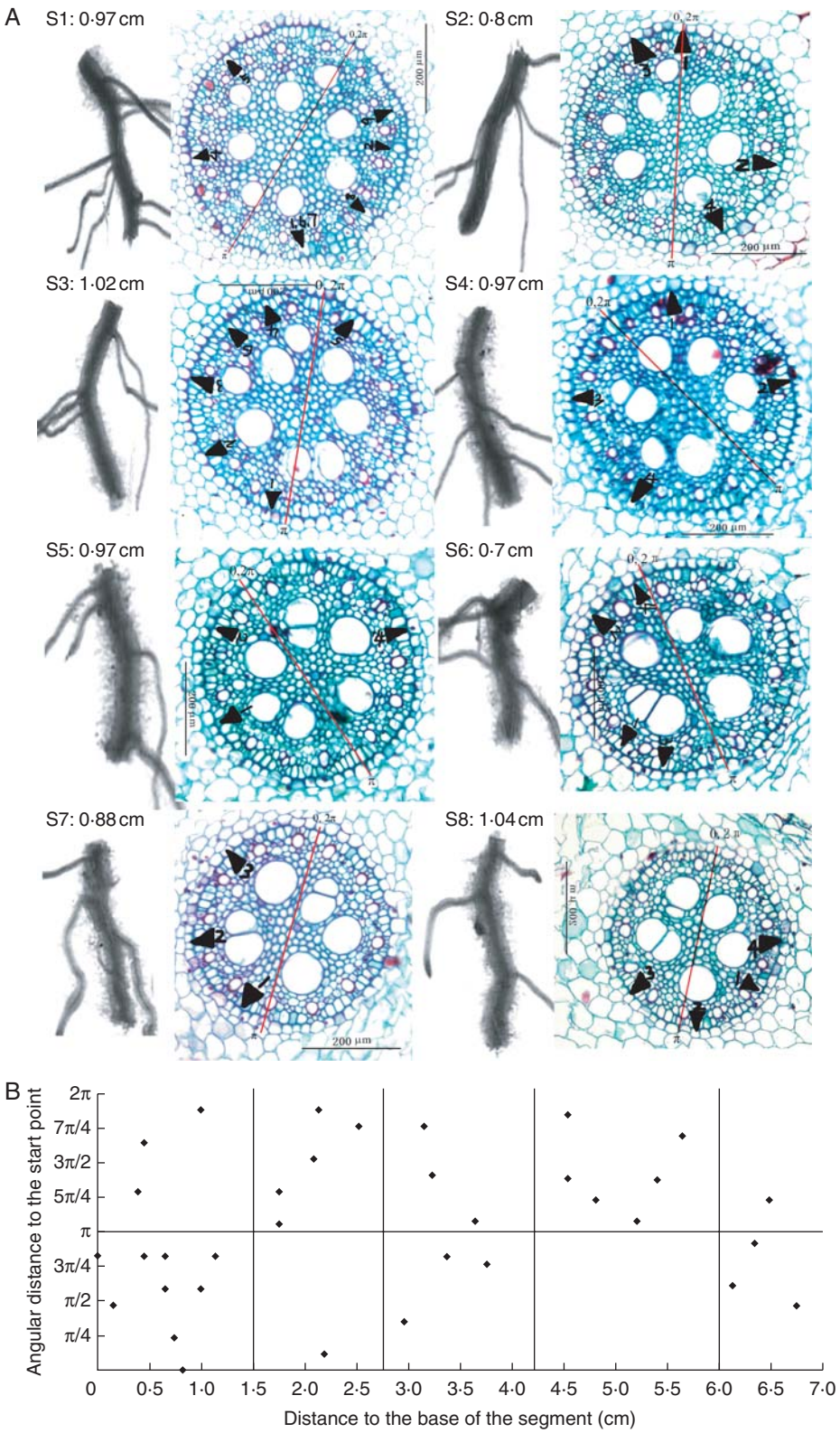

FIG. 7. Spatial arrangements of lateral roots along nodal root axis. (A) Projections of lateral roots on the transverse plane (black triangles). A 7-cm-long root was cut into eight segments labelled s1–s8, with s1 being the most proximal (nearest to the root base), and s8 the most distal (nearest to the root tip). Scan pictures and the corresponding cross-section images of each segment are lined up. The values following the segment codes are their respective lengths. Note that most lateral roots occur on the convex side of the mother root. Numbers following the black triangles indicate the sequence of the lateral roots on the segment in the direction of root base to tip. (B) The radial and axial distribution of lateral roots. Over short distances (within the two vertical lines), lateral roots tend to cluster on one side of a transverse plane, but over longer distances, there is a tendency for a more uniform distribution. See Fig. 2 for the labelling of lateral root position on the mother roots. The red lines in the cross-sections serve as the starting points (0, 2π) and central axes for aligning the serial sections.

has the advantage that it is based on a classical, serial-section method that does not involve costly and sophisticated equipment such as confocal microscopes and CT. In addition, the tissue arrangement along the root axis can be expressed both qualitatively and quantitatively.

Using the 3-D reconstruction and visualization technique developed here, the spatial arrangement of the structures in both radial and longitudinal directions could be illustrated simultaneously, with the evolution of the internal structures along the root axis reflecting developmental progression. As the passage cells and lateral roots are constituents of the radial pathway of water and nutrient transport, and the linkage of xylem vessels forms the axial pathway, the spatial relationships among these structures depicted by the technique illustrate both the spatial relationship between radial and axial transport pathways and the temporal evolution of this relationship. The frequent transition and the evolution of the number and diameter of xylem vessels along the root axis resulted in a balance between maintaining efficiency for water and nutrient transport and risk-mitigation against embolism and pathogen invasion. Passage cell numbers decreased drastically as root segments matured; in old root segments they were partially replaced by (and coexisted with) lateral roots, mirroring their similar functions as radial passages for water and nutrient transport to the stele. The results demonstrated the close synchronization and spatial co-ordination among root anatomy structures that are essential for the radial and axial transport of water and nutrients from the soil solution to the shoot.

It has to be acknowledged that our technique suffered the drawback of being rather time consuming, thus the length of root segments that can be examined is very limited. To illustrate better the relationship between passage cells and lateral roots along the root axis, it would be desirable to perform reconstructions in longer root segments using a hand-cut method. Moreover, the presence of lateral roots makes transverse sectioning and alignment difficult. Our technique is thus a compromise between a requirement for relatively unsophisticated equipment on the one hand, but time-consuming labour on the other. As fixation peparation in the paraffin sections kills cells, this also prevents analysis of the viability and functioning of the cells. In the future, we aim to combine our technique with cryo-microscopy in order to investigate the nature of the pericycle cells adjacent to the passage cells and to elucidate positional effects in the building of the root anatomical structure.

ACKNOWLEDGEMENTS

This work was supported by a project of the National High Technology of Research and Development of China (grant no. 2003AA209020) of the Chinese Ministry of Science and Technology as well as by the LIAMA 'Greenlab' project. We thank Dr Alexander Lang for constructive remarks and suggestions.

LITERATURE CITED

Aloni R. 1992. The control of vascular differentiation. *Journal of Plant Science* **153**: S90–S92.

Aloni R. 2004. The induction of vascular tissue by auxin. In: Davies PJ, ed. *Plant hormones: biosynthesis, signal transduction, action.* Berlin: Springer.

Aloni R, Zimmermann MH. 1983. The control of vessel size and density along the plant axis: a new hypothesis. *Differentiation* **24**: 203–208.

Aloni R, Aloni E, Langhans M, Ullrich CI. 2006. Role of cytokinin and auxin in shaping root architecture: regulating vascular differentiation, lateral root initiation, root apical dominance and root gravitropism. *Annals of Botany* **97**: 883–893.

Bardage LS. 2001. Three-dimensional modeling and visualization of whole Norway spruce latewood tracheids. *Wood and Fiber Science* **33**: 627–638.

Casimiro I, Marchant A, Bhalerao RP, *et al*. 2001. Auxin transport promotes Arabidopsis lateral root initiation. *The Plant Cell* **13**: 843–852.

Cloetens P, Mache R, Schlenker M, Lerbs-Mache S. 2006. Quantitative phase tomography of Arabidopsis seeds reveals intercellular void network. *Proceedings of the National Academy of Sciences of the USA* **103**: 14626–14630.

Cholewa E, Peterson CA. 2004. Evidence for symplastic involvement in the radial movement of calcium in onion roots. *Plant Physiology* **134**: 1793–1802.

De Smet I, Vanneste S, Inzé D, Beeckman T. 2006. Lateral root initiation or the birth of a new meristem. *Plant Molecular Biology* **60**: 871–887.

De Smet I, Tetsumura T, De Rybel B, *et al*. 2007. Auxin-dependent regulation of lateral root positioning in the basal meristem of Arabidopsis. *Development* **134**: 681–690.

Dubrovsky JG, Doerner PW, Colón-Carmona A, Rost TL. 2000. Pericycle cell proliferation and lateral root initiation in Arabidopsis. *Plant Physiology* **124**: 1648–1657.

Eils R, Athale C. 2003. Computational imaging in cell biology. *Journal of Cell Biology* **161**: 477–481.

Enquist BJ, West GB, Brown JH. 2000. Quarter-power allometric scaling in vascular plants: functional basis and ecological consequence. In: Brown JH, West GB, eds. *Scaling in biology*. New York, NY: Oxford University Press, 167–198.

Fang SQ, Yan XL, Liao H. 2009. 3-D reconstruction and dynamic modeling of root architecture *in situ* and its application to crop phosphorus research. *The Plant Journal* **60**: 1096–1108.

Gerlich D, Beaudouin J, Kalbfuss B, Daigle N, Eils R, Ellenberg J. 2003. Global chromosome positions are transmitted through mitosis in mammalian cells. *Cell* **112**: 751–764.

Grieneisen VA, Xu J, Marée AFM, Hogeweg P, Scheres B. 2007. Auxin transport is sufficient to generate a maximum and gradient guiding root growth. *Nature* **449**: 1008–1013.

Hartman J, Wernecke J. 1996. *The VRML 2·0 handbook: building moving worlds on the web*. Redwood City, CA: Addison Wesley Longman Publishing Co.

Johansen DA. 1940. *Plant microtechnique*. New York, NY: McGraw-Hill.

Kaestner A, Schneebeli M, Graf F. 2006. Visualizing three-dimensional root networks using computed tomography. *Geoderma* **136**: 459–469.

Lee K, Avondo J, Morrison H, *et al*. 2006.. Visualizing plant development and gene expression in three dimensions using optical projection tomography. *The Plant Cell* **18**: 2145–2156.

Lin JX, Lin YH, Yang HD. 1997. Reconstruction of xylem longitudinal water conducting networks with serial section and computer-aided image superposition techniques. *Chinese Science Bulletin* **42**: 330–332.

Lontoc-Roy M, Dutilleul P, Prasher SO, Smith DL. 2004. 3-D visualization and quantitative analysis of plant root systems using helical CT scanning. In: Godin C, Hanan J, Kurth W *et al*., eds. *Proceedings of the Fourth International Workshop on Functional–Structural Plant Models*, 13–16. http://amap.cirad.fr/workshop/ FSPM04/index.html.

Lontoc-Roy M, Dutilleul P, Prasher S, Han L, Smith DL. 2005. Computed tomography scanning for three-dimensional imaging and complexity analysis of developing root systems. *Canadian Journal of Botany* **83**: 1434–1442.

Lucas M, Godin C, Jay-Allemand C, Laplaze L. 2008. Auxin fluxes in the root apex co-regulate gravitropism and lateral root initiation. *Journal of Experimental Botany* **59**: 55–66.

Lux A, Luxová M. 2003. Growth and differentiation of root endodermis in *Primula acaulis* Jacq. *Biologia Plantarum* **47**: 91–97.

Ma F, Peterson CA. 2001. Development of cell wall modifications in the endodermis and exodermis of *Allium cepa* roots. *Canadian Journal of Botany* **79**: 621–634.

Ma FS, Peterson CA. 2003. Current insights into the development, structure, and chemistry of the endodermis and exodermis of root. *Canadian Journal of Botany* **81**: 405–421.

Ma Y. 1999. *Wheat root*. Beijing: Agriculture Publishing Company.

Mallory TE, Chiang S, Cutter EG, Gifford EM. 1970. Sequence and pattern of lateral root formation in five selected species. *American Journal of Botany* **57**: 800–809.

Mayo SC, Chen F, Evans R. 2010. Micron-scale 3-D imaging of wood and plant microstructure using high-resolution X-ray phase-contrast microtomography. *Journal of Structural Biology* **171**: 182–188.

North GB. 2004. A long drink of water: how xylem changes with depth. *New Phytologist* **163**: 447–449.

Peterson CA, Enstone DE. 1996. Functions of passage cells in the endodermis and exodermis of roots. *Physiologia Plantarum* **97**: 592–598.

Prudhomme M, Gaubert-Cristol R, Jaeger M, de Reffye P, Godlewski G. 1999. A new method of three-dimensional computer assisted reconstruction of the developing biliary tract. *Journal of Clinical Anatomy* **21**: 55–58.

de Reuille PB, Bohn-Courseau I, Godin C, Traas J. 2005. A protocol to analyse cellular dynamics during plant development. *The Plant Journal* **44**: 1045–1053.

Romheld V, Marschner H. 1986. Evidence for a specific uptake system for iron phytosiderophores in roots of grasses. *Plant Physiology* **80**: 175–180.

Simionovici A, Chukalina M, Günzler F, *et al.* 2001. X-ray microtome by fluorescence tomography. *Nuclear Instruments and Methods in Physics Research A* **467/468**: 889–892.

Sperry JS, Hacke UG. 2002. Desert shrub water relations with respect to soil characteristics and plant functional type. *Functional Ecology* **16**: 367–378.

Steudle E, Peterson C. 1998. How does water get through roots? *Journal of Experimental Botany* **49**: 775–788.

Stuppy WH, Maisano JA, Colbert MW, Rudall PJ, Rowe TB. 2003. Three-dimensional analysis of plant structure using high-resolution X-ray computed tomography. *Trends in Plant Science* **8**: 2–6.

Tracy SR, Roberts JA, Black CR, McNeill A, Davidson R, Mooney SJ. 2010. The X-factor: visualizing undisturbed root architecture in soils using X-ray computed tomography. *Journal of Experimental Botany* **61**: 311–313.

Truernit E, Bauby H, Dubreucq B, *et al.* 2008. High-resolution whole-mount imaging of three-dimensional tissue organization and gene expression enables the study of phloem development and structure in *Arabidopsis*. *The Plant Cell* **20**: 1494–1503.

Tyree MT, Ewers FW. 1991. The hydraulic architecture of trees and other woody plants. *New Phytologist* **119**: 345–360.

Waduwara CI, Walcott SE, Peterson CA. 2008. Suberin lamellae of the onion root endodermis: their pattern of development and continuity. *Canadian Journal of Botany* **86**: 623–632.

West GB, Brown JH, Enquist BJ. 1999. A general model for the structure and allometry of plant vascular systems. *Nature* **400**: 664–667.

Wu H, Jaeger M, Wang M, Li B, Zhang BG. 2009. Three-dimensional reconstruction and visualization of xylem vessels of wheat nodal root. PMA. *Third International Symposium on Plant Growth Modeling, Simulation, Visualization and Applications*, 384–390. http://doi.ieeecomputersociety.org/10.1109/PMA.2009.39.

Zimmermann MH. 1983. *Xylem structure and the ascent of sap.* Berlin: Springer-Verlag.

Zhu T, Tian F, Zhou Y, Seah HS, Yan X. 2008. Plant modeling based on 3d reconstruction and its application in digital museum. *The International Journal of Virtual Reality* **7**: 81–88.